RESEARCH ARTICLE

Formulation and evaluation of a bioink composed of alginate, gelatin, and nanocellulose for meniscal tissue engineering

Julia Anna Semba[1,2], Adam Aron Mieloch[1], Ewa Tomaszewska[3], Piotr Cywoniuk[1], Jakub Dalibor Rybka[1]*

[1]Center for Advanced Technology, Adam Mickiewicz University, Poznan, Poland

[2]Faculty of Biology, Adam Mickiewicz University, Poznan, Poland

[3]Faculty of Mechanical Engineering, Poznan University of Technology, Poznan, Poland

*Corresponding author:
Jakub Dalibor Rybka
(jrybka@amu.edu.pl)

Abstract

The necessity to preserve meniscal function prompts the research and development of novel treatment options, like three-dimensional (3D) bioprinting. However, bioinks for meniscal 3D bioprinting have not been extensively explored. Therefore, in this study, a bioink composed of alginate, gelatin, and carboxymethylated cellulose nanocrystal (CCNC) was formulated and evaluated. Firstly, bioinks with varying concentrations of the aforementioned components were subjected to rheological analysis (amplitude sweep test, temperature sweep test, and rotation). The optimal bioink formulation of 4.0% gelatin, 0.75% alginate, and 1.4% CCNC dissolved in 4.6% D-mannitol was further used for printing accuracy analysis, followed by 3D bioprinting with normal human knee articular chondrocytes (NHAC-kn). The encapsulated cells' viability was > 98%, and collagen II expression was stimulated by the bioink. The formulated bioink is printable, stable under cell culture conditions, biocompatible, and able to maintain the native phenotype of chondrocytes. Aside from meniscal tissue bioprinting, it is believed that this bioink could serve as a basis for the development of bioinks for various tissues.

1. Introduction

Meniscal lesions are one of the most common injuries to the human knee, stemming from its biomechanical role as a shock absorber[1]. The clinical results of meniscus repair have direct correlations with the vascularization of the area in which the lesion occurs. The vascularized zone has higher regenerative potential in comparison to the avascular zone. The routine treatment methods include stitching and partial meniscectomy, which pose a risk of detachment and limitation to joint mobility[2,3]. There is also a risk of late-age osteoarthritis with meniscectomy, as it decreases the contact area and increases the contact stress on the articular cartilage. In the case of complex and extensive meniscal tears, the treatment options include allograft transplantation; however, tissue

accessibility is a major limitation. Therefore, cartilage regeneration or substitute through a tissue-engineered scaffold is extensively explored.

Three-dimensional (3D) bioprinting emerges as a versatile method to manufacture structurally defined constructs[4]. In short, 3D bioprinting utilizes a carrier matrix termed bioink to provide a microenvironment for cells suspended within it[5]. The main advantage of 3D bioprinting is the architectural control over products[6]. A perfectly tailored scaffold can be developed using data from various imaging techniques, like magnetic resonance imaging (MRI)[7]. The growing interest in this field of research is anticipated[8]. Presently, 3D bioprinting is used to manufacture tissues, organs, or cancer models for research, including orthopedic applications[9].

Literature presents various bioink compositions developed for orthopedic 3D bioprinting[5]. An interesting idea is to formulate bioink based solely on the decellularized extracellular matrix (ECM) from porcine menisci[10,11]. This low immunogenic component exhibits good biocompatibility and stimulates chondrogenesis. However, constructs suffer from poor mechanical stability, which is an issue that has to be addressed. Polycaprolactone (PCL) is frequently used as a reinforcement in orthopedic applications[12,13]. For example, PCL supports alginate-based bioinks mixed with porcine inner or outer meniscal ECM[10,14]. Nevertheless, ECM extraction requires the use of surfactants that may elicit cytotoxic effects even at low concentrations[15]. Alternative methods of supercritical carbon dioxide (CO_2) extraction require advanced and costly equipment. As a result, alginate, collagen derivatives, chitosan, nanocellulose, and hyaluronic acid are some of the more widely investigated biomaterials[5].

The most commonly used bioink component is an accessible and affordable alginate that crosslinks with divalent cations, usually calcium ions (Ca^{2+}). Nonetheless, the rapid alginate gelation limits the control over this process during bioprinting[16]. Therefore, it is usually mixed with other materials, like gelatin, to obtain bioinks with dual-stage gelation[7]. The gelation of gelatin is temperature-dependent; it is fluid above 30°C but solid at lower temperatures. In addition, gelatin, unlike alginate, has a positive charge that ensures cell and protein binding[17]. Alginate-gelatin bioink is commonly used as a basis for bone and cartilage tissue engineering[18–20].

In cartilage-related research, the addition of nanocellulose enhances the mechanical properties and shear forces affecting cells and printability[7,21,22]. The cell mobility inside constructs and phenotypic changes are related to the mechanical properties of bioink[23]. Cells detect mechanical stress through mechanoreceptors, which convert mechanical stimuli into biochemical signals that regulate various cellular pathways[24]. The mechanical stimulation is further enhanced by shear forces exerted on cells during 3D bioprinting[7,25]. This phenomenon is known as mechanotransduction and is one of the chondrogenesis stimulators.

Extrusion-based bioprinting, which is the most popular type of bioprinting, utilizes compressed air or a mechanical piston to extrude bioink from a cartridge[5,26]. It is a relatively affordable technique and is compatible with various materials, including alginate- and gelatine-based bioinks[27,28]. The applicability of extrusion-based bioprinting can be expanded by integrating additional modules, such as the microfluidic printhead or the UV module for photo-curable materials[29,30]. Inkjet bioprinting is another 3D bioprinting technology that ejects droplets; hence, it allows the manufacturing of constructs in a drop-on-demand fashion[31,32]. Laser-assisted bioprinting systems, such as laser-induced forward transfer (LIFT) and vat polymerization-based bioprinting, can also be used as 3D bioprinting techniques for cartilage tissue engineering. LIFT is a nozzle-free and noncontact technique that is applicable for high-viscosity bioinks with high cell densities[5]. The laser is pulsed on a ribbon that absorbs energy and generates a bubble of bioink on the opposite side[5,33]. Vat polymerization is based on the polymerization of photo-curable inks in vats and is mainly used for 3D printing with inks without cells. Nevertheless, digital light processing is a vat polymerization technology that has been successfully used for bioprinting with bioinks mixed with cells[34,35]. A bioink composed of alginate, gelatin, and carboxymethylated cellulose nanocrystal (CCNC) was formulated and evaluated for meniscal tissue engineering. The addition of CCNC is a novelty selected for its carboxymethylated groups that increase its solubility. All materials are natural, biocompatible, accessible, and affordable. Rheological analysis was performed on bioinks with varying concentrations of alginate, gelatin, and CCNC. Based on the rheological analysis, a bioink was selected for printing accuracy analysis, and the bioink was subsequently enriched with normal human knee articular chondrocytes (NHAC-kn) for 3D bioprinting. The constructs were created with an extrusion-based bioprinter. The viability and gene expression of the embedded cells were assessed.

2. Materials and methods

2.1. Bioink preparation for rheological analysis

Table 1 presents the investigated bioink formulations. Firstly, weighted sodium alginate (Sigma-Aldrich), gelatin from porcine skin (Sigma-Aldrich), and CCNC (Cellulose Lab) were sterilized under ultraviolet (UV) light for 30 minutes. The components were then dissolved in

Table 1. Bioink formulations for rheological analysis

	Concentrations (w/v)		
	Gelatin	Alginate	CCNC
Bioink A	3.0%	0.5%	1.4%
Bioink B	4.0%	0.5%	1.4%
Bioink C	5.0%	0.5%	1.4%
Bioink D	4.0%	0.75%	1.4%
Bioink E	4.0%	1.0%	1.4%
Bioink F	4.0%	0.75%	1.0%
Bioink G	4.0%	0.75%	2.0%

Abbreviation: CCNC, carboxymethylated cellulose nanocrystal.

sterile 4.6% (w/v) D-mannitol (Sigma-Aldrich) solution. The components were added in the following order: alginate, gelatin, and CCNC; the mixture was shaken after each addition for at least 30 minutes at 37°C. The prepared bioinks were mixed overnight. During bioink formulation, the EFD Optimum dispensing equipment (Nordson) ensures a high repeatability of bioink composition by wiping the residues from the walls with a piston.

2.2. Rheological analysis

Rheological analysis was performed using the Anton Paar 302 rheometer, equipped with 25 mm, smooth, parallel plates (PP25). The gap between plates was set to 1 mm, and measurements were conducted at 23°C, unless stated otherwise. The performed rheological measurements included amplitude sweep test, temperature sweep test, and rotation. Temperature sweep experiments were performed at a rate of 2°C·min^{-1} from 20°C to 40°C. In the rotation study, the shear rate range was set to 0.01–200.00 s^{-1}. The oscillatory measurement was divided into three intervals[36]. The first interval was a pre-shear step conducted at a constant strain amplitude (γ) of 0.01% and an angular frequency (ω) of 10 s^{-1}. The next interval was a rest time (t = 10 minutes), followed by an amplitude sweep test with varying strain amplitude (0.01%–500.00%) and a constant angular frequency (1 rad·s^{-1}). A layer of silicone oil was spread over the surface of the sample to prevent water evaporation from the bioink samples during rheological measurements[36,37]. All rheological measurements were performed in triplicate, including sample preparation, and at least three measurements were performed for further calculations.

2.3. 3D model design

Three computer-aided design (CAD) models were developed. The first model was developed for printing accuracy analysis, while the second model was developed to test the feasibility of bioprinting a meniscus-like shape model (approximately 29 mm × 39 mm × 11 mm). Both were prepared with Inventor Professional 2020. The

stereolithography (STL) models were adjusted based on the bioprinter requirements in Slic3r. The third model (10 mm × 10 mm × 1 mm cylinder) was less challenging, and it was prepared using Thinkercad for 3D bioprinting. This model was uploaded to the BIO X bioprinter (Cellink) and sliced using a bioprinting software with infill set at a 35% rectilinear pattern.

2.4. Printing accuracy analysis

The bioink selection for 3D bioprinting accuracy analysis was based on the former rheological analysis. The bioink was prepared as described above, transferred to a cartridge, and precooled in a 25°C water bath. The BIO X bioprinter (Cellink) with temperature-controlled, pressure extrusion printhead was used. Its printhead and printbed temperatures were set to 25°C and 10°C, respectively. A 22 G needle (inner diameter = 410 μm) was used. After printing, the constructs were photographed on millimeter paper, and all measurements were taken from 15 individually printed constructs. The length and width measurements for printing accuracy were performed on ImageJ software. The printing accuracy in percentage was assessed with a previously proposed equation[38] as follows:

$$Printing\,accuracy\left[\%\right]=\left[1-\frac{\left|A_i\left[mm\right]-A\left[mm\right]\right|}{A\left[mm\right]}\right]*100$$

where A_i is the measurement of a printed construct, and A is the measurement of a 3D model.

2.5. Culture of NHAC

Normal human knee articular chondrocytes (NHAC-kn, Lonza) were cultured in the recommended CGM™ Chondrocyte Growth Medium (Lonza) for expansion of chondrocytes, with supplementation at standard conditions (37°C, 5% CO$_2$, and 95% relative humidity). Cell passaging was performed with TrypLE™ Express Enzyme (Gibco) when the cells reached 80%–90% confluence. Chondrocytes up to the sixth passage were used for 3D bioprinting.

2.6. Bioink preparation for 3D bioprinting

The bioink prepared as described above was further mixed by using two syringes clipped with the female/female luer lock adapter. The prepared bioink was mixed with 1 × 10^7 cells·mL^{-1} of bioink in the same way. Specifically, the cells were suspended in 100 μL of chondrocyte medium and transferred to a syringe, while 1 mL of bioink was transferred to another syringe; then, the syringes were clipped with a female/female luer lock adapter prior to mixing the content. Before bioprinting, the bioink with cells was placed in a cartridge and held in a 25°C water bath to induce gelatin gelation.

2.7. 3D bioprinting

The 3D bioprinting proceeded with the same parameters as those in the printing accuracy analysis; the only difference was the printing nozzle, which was 25 G. After bioprinting, the constructs were crosslinked with sterile 200 mM calcium chloride (CaCl$_2$) (Sigma-Aldrich) dissolved in 4.6% (w/v) D-mannitol for 10 minutes at room temperature. Then, the constructs were cultured in supplemented CGM™ Chondrocyte Growth Medium with 5 mM CaCl$_2$ in standard conditions.

2.8. Live/dead assay

After 24 h, 7 days, 14 days, and 28 days, three bioprinted constructs were divided for viability and gene expression analyses. The live/dead assay was performed according to the product manual (LIVE/DEAD® Viability/Cytotoxicity Kit, Invitrogen), with the utilization of confocal microscopy (IX83, Olympus). Scans for viability assessment were taken from the approximate midpoint of three different constructs at each time point. From each of these scans, two middle slices were selected for live and dead cell counting. These images were analyzed with the ImageJ software.

2.9. Gene expression analysis

Three constructs from each time point were dissolved in 100 mM sodium citrate, containing 0.08 U·µL^{-1} Proteinase K and 1.0 U·µL^{-1} RNAse Inhibitor (A&A Biotechnology), while shaking for 5 minutes at 37°C, followed by ribonucleic acid (RNA) isolation with TriReagent (Sigma-Aldrich). Chloroform was then added, and the probes were centrifuged at 12,000 RCF for 15 minutes at 4°C. The supernatant was collected and mixed with a 1:1 volume of cold 99% ethanol. The solution was then transferred to the columns from RNeasy Mini Kit. The isolation steps were performed according to the RNeasy Mini Kit manual. The RNA concentration was measured using the Qubit 4 Fluorometer. For reverse transcription polymerase chain reaction (RT-PCR), TranScriba Kit (A&A Biotechnology) was used with random hexamer primers and 300 ng of total RNA. The following genes for real-time PCR were selected: *COL1A1*, *COL2A1*, *COL10A1*, *SOX9*, and *RUNX2*, with *GAPDH* as the housekeeping gene. The

Table 2. Primer sequences used for gene expression analysis

Gene name	Forward/Reverse	Sequence
COL1A1	F	5'-ACGTCCTGGTGAAGTTGGTC-3'
	R	5'-ACGTCCTGGTGAAGTTGGTC-3'
COL2A1	F	5'-CTGGAAAAGATGGTCCCAAAG-3'
	R	5'-CAGGGAATCCTCTCTCACCAC-3'
COL10A1	F	5'-TTACGCTGAACGATACCAAATG-3'
	R	5'-GACTTCCGTAGCCTGGTTTTC-3'
SOX9	F	5'-GACTCGCCACACTCCTCCT-3'
	R	5'-AGGTCTCGATGTTGGAGATGAC-3'
RUNX2	F	5'-ACCAGATGGGACTGTGGTTACT-3'
	R	5'-TGTGAAGACGGTTATGGTCAAG-3'
GAPDH	F	5'-TGACATCAAGAAGGTGGTGAAG-3'
	R	5'-TTCGTTGTCATACCAGGAAATG-3'

designed starters are shown in Table 2. The QuantStudio 6k Flex Real-Time PCR System (Applied Biosystems) with 1 µL of complementary deoxyribonucleic acid (cDNA) and Maxima SYBR Green/ROX qPCR Master Mix (Thermo Scientific) was used to evaluate the expression of these genes. Primers were used at a final concentration of 0.5 µM. The gene expression results were tested with the two-way analysis of variance (ANOVA).

2.10. Data analysis

GraphPad Prism 8.0.1 was used for statistical computing and graph preparation.

3. Results

3.1. Rheology

The temperature sweep test compared the storage modulus (G'), the loss modulus (G"), and the cross-over temperature (G' = G") between bioink A, B, and C (Figure 1). G'/G" cross-over indicates the temperature at which the bioink changes its state. If G' is above G", the elastic part dominates in the viscoelastic spectrum, and the bioink is solid. Conversely, if G" is above G', the viscous part dominates,
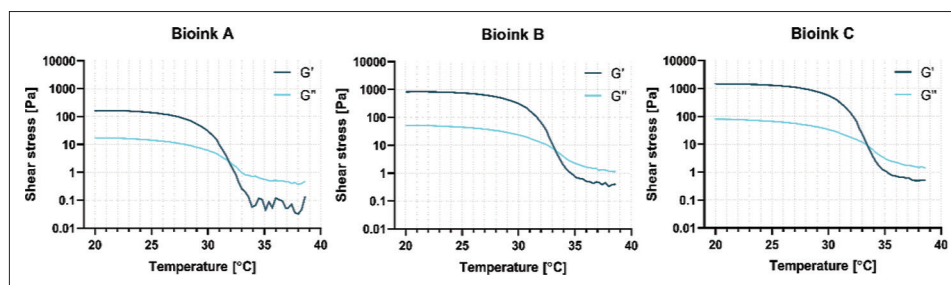

Figure 1. The temperature-dependent functions of storage modulus G' and loss modulus G" of bioinks A, B, and C.
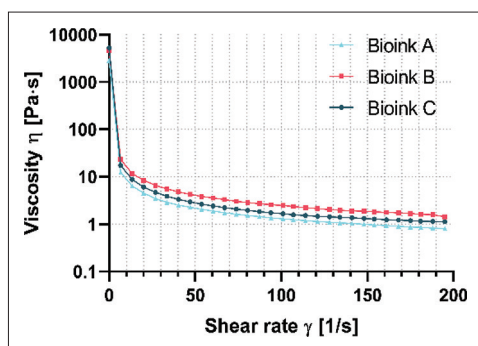
Figure 2. Flow curves of bioinks A, B, and C.

and the bioink is liquid. Bioink A reached its lowest G'/G" at 32.3°C. Bioinks B and C obtained similar G'/G" values at 33.1°C and 33.3°C, respectively. These bioinks also had higher values of both, storage and loss modulus, particularly in the temperature range of 20°C to 35°C.

Bioink flow analysis with gelatin content from 3.0% to 5.0% enables the estimation of printability (Figure 2). All bioinks exhibited a shear-thinning behavior, in which shear rate (γ) increases and shear stress (τ) decreases viscosity (η). In the conducted research, the viscosity range for all bioinks was similar. It was 2863–0.08 Pa·s for bioink A, 4630–0.02 Pa·s for bioink B, and 5210–0.05 Pa·s for bioink C at a shear rate range of 0.01–200.00 s^{-1}.

In the amplitude sweep test, bioinks with varying concentrations of each component were tested, beginning with bioinks with different gelatin content (3.0%, 4.0%, and 5.0%) (Figure 3). All bioinks displayed a solid-like

behavior (G' > G") until G'/G" cross over. Expectedly, a lower gelatin content corresponded to the cross-over at lower strain rates, while higher gelatin content resulted in higher values of G'. Hydrogels with 3.0% and 5.0% of gelatin showed a slight increase in the storage modulus followed by a steep downward slope. From the above results, the gelatin content was set at 4.0%.

Subsequently, amplitude sweep tests were performed on bioinks with varying alginate content (0.5%, 0.75%, and 1.0 %) (Figure 4). Bioink B revealed the highest constancy in G' values resulting in a broad linear viscoelastic (LVE) region. Interestingly, bioinks D and E with higher alginate content revealed a similar spike in G' as observed for bioinks A and C. Bioinks B, D, and E reached G'/G" crossover at 239%, 340%, and 396% strain, respectively. The 0.75% alginate content was selected for further analysis.

The next step involved testing bioinks with fixed gelatin (4.0%) and alginate (0.75%) contents but varying CCNC concentrations (bioink D, 1.4%; bioink F, 1.0%; and bioink G, 2.0%) using the amplitude sweep test (Figure 5). There was a significant increase in G' with increasing CCNC concentration, but the increase in G" was less noticeable. This could be explained by the hydrophilic properties of CCNC that contribute to an overall increase in the solid component of the bioinks, resulting in elevated G'. Bioinks F, D, and G reached the G'/G" crossover at 366%, 340%, and 256% strain, respectively, demonstrating the improvement of shear-thinning properties with the addition of CCNC.
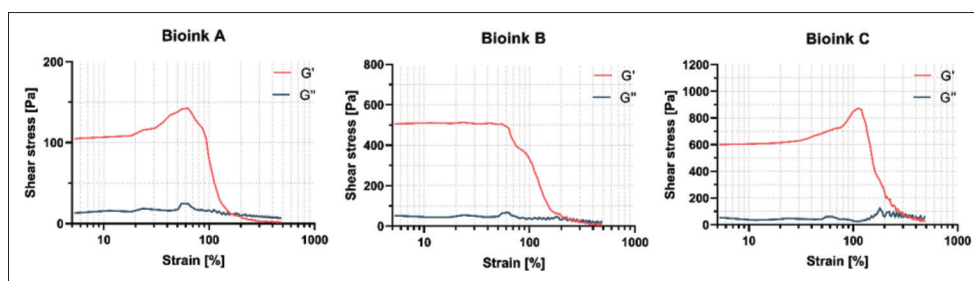

Figure 3. The results of amplitude sweeps of bioinks A, B, and C (increasing gelatin content: 1.0%, 1.4%, 2.0%).
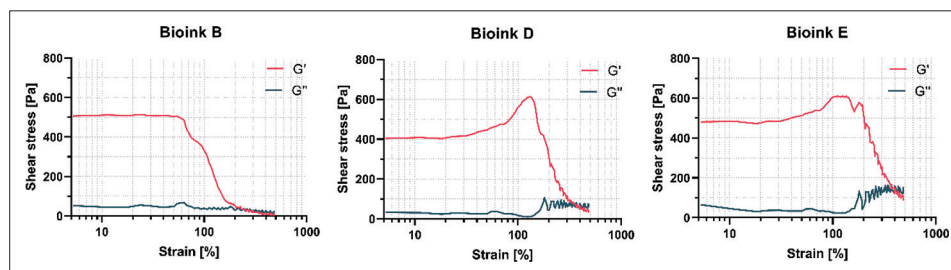

Figure 4. The results of amplitude sweeps of bioinks B, D, and E (increasing alginate content: 0.5%, 0.75%, 1.0%).
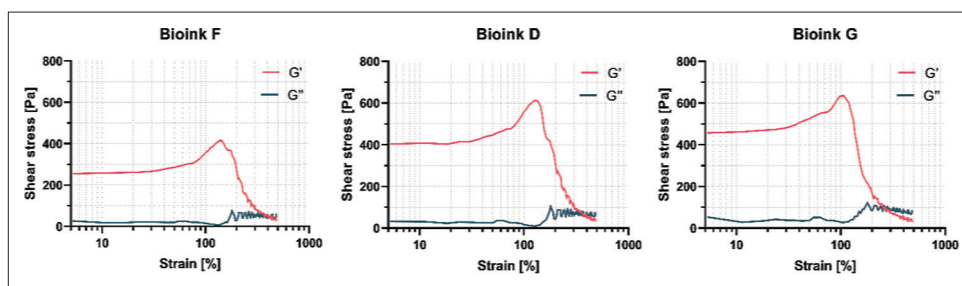
Figure 5. The results of amplitude sweeps of bioinks F, D, and G (increasing CCNC content: 1.0%, 1.4%, 2.0%).
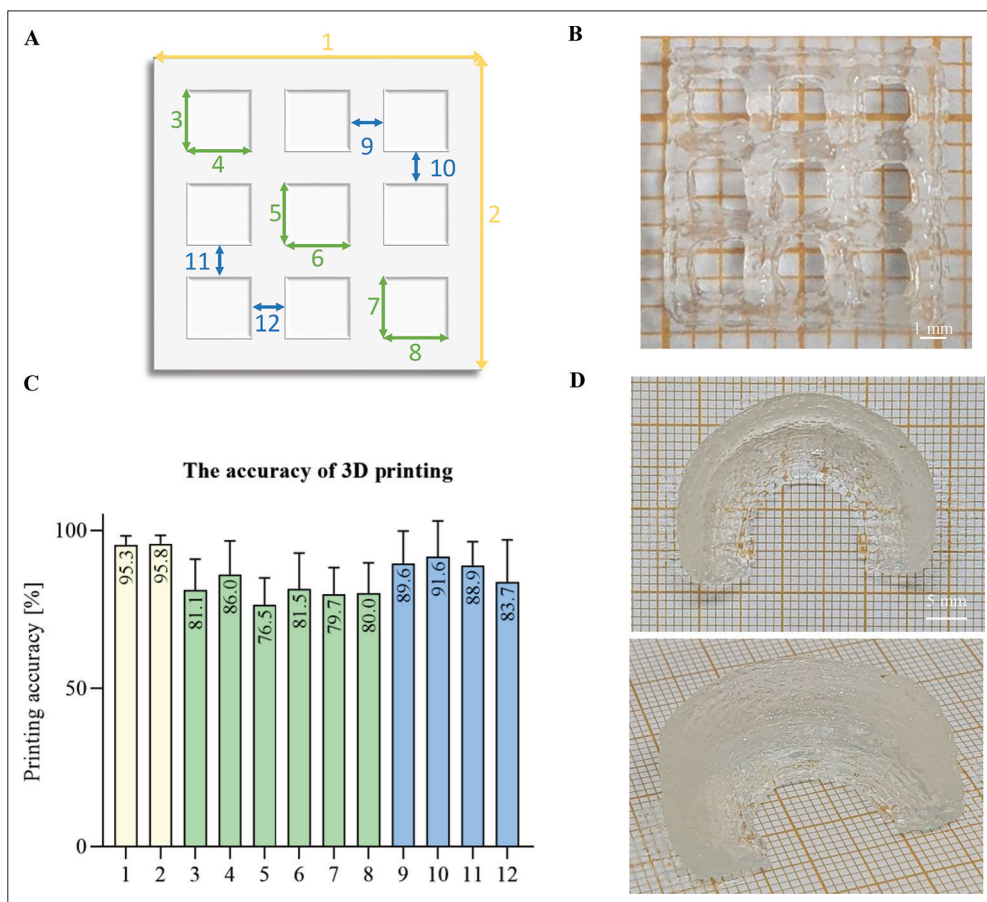

Figure 6. The accuracy of 3D printing with 0.75% alginate_4.0% gelatin_1.4% CCNC bioink without cells. (A) Measured dimensions for calculating the accuracy of 3D printing. (B) A representative image of the printed construct used for calculating the accuracy of 3D printing. (C) The accuracy of 3D printing. The colors of columns correspond to the colors in A; consequently, yellow indicates the measurements outside, green indicates the measurements inside the holes, and blue indicates the measurements within the walls. (D) A bioprinted meniscus-like shape model.

The bioink with 4.0% gelatin, 0.75% alginate, and 1.4% CCNC (Bioink D) was selected for further analysis.

3.2. Printing accuracy

The printing accuracy of constructs developed with bioink D was compared to the CAD model (Figure 6A and B). The best accuracy was obtained with a 25 G nozzle that operates at 40–55 kPa with a speed of 22–30 mm·s⁻¹. We observed a steady flow of bioink through the 25 G nozzle, contrary to the clogged 27 G nozzle. The measurements outside (dimensions 1 and 2, Figure 6A) were approximately 96.0% accurate (Figure 6C). Inside the walls, a similarly high level of accuracy (between 92.5% and 97.1%) was obtained (dimensions from 9 to 12, Figure 6A and C). The lowest accuracy with the highest deviations was observed for measurements inside the holes (dimensions from 3 to 8,
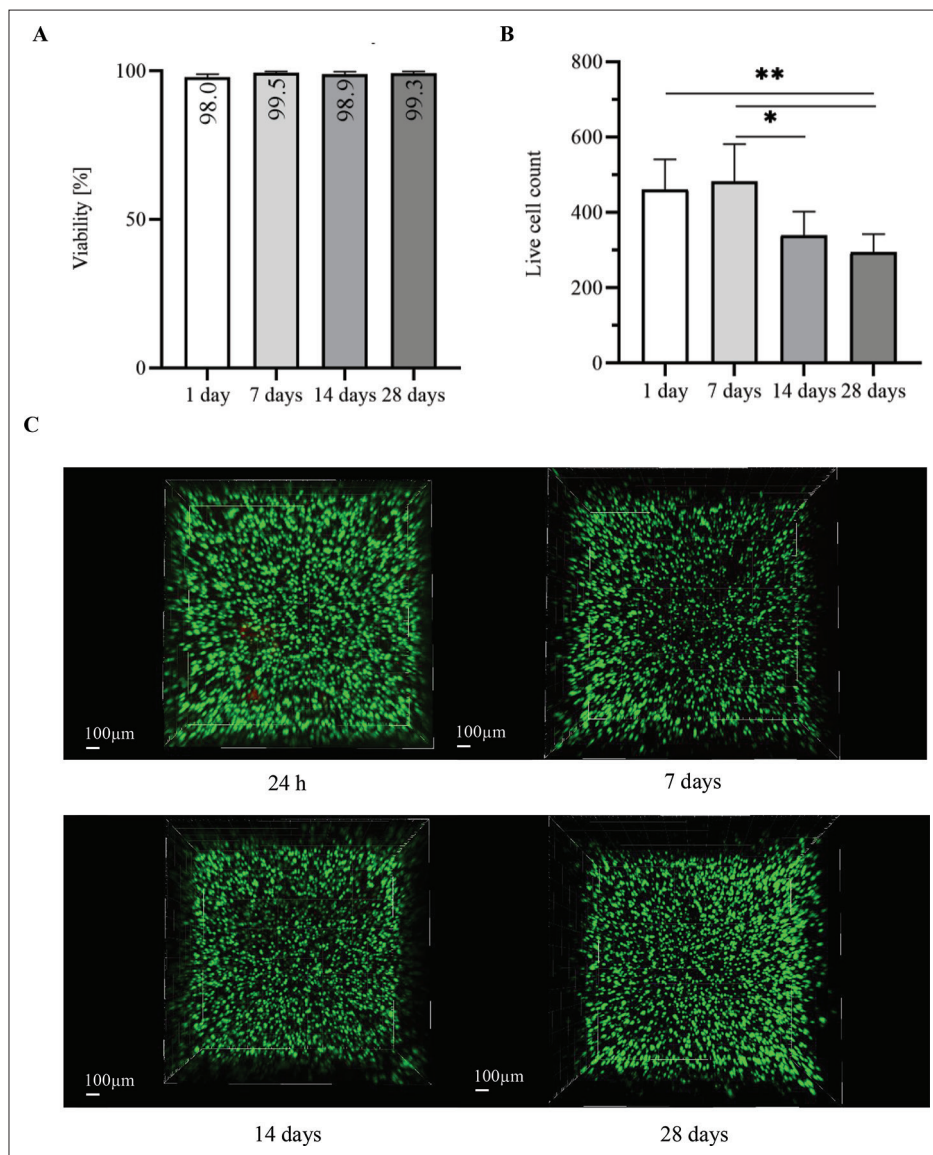
Figure 7. Viability of normal human knee articular chondrocytes (1×10^7 cells·mL^{-1}) bioprinted with 0.75% alginate_4.0% gelatin_1.4% CCNC bioink assessed by LIVE/DEAD assay (Invitrogen). (A) Viability at different time points. (B) Changes in cell count during culture. Note: *P value ≤ 0.05; **P value ≤ 0.02. (C) Representative 3D confocal scans from the constructs.

Figure 6A and C). The meniscus-like shape model was also bioprinted (Figure 6D).

3.3. Cell viability

The cell viabilities at all time points were above 98% (Figure 7A); however, there was a significant drop in cell count after one week (Figure 7B). Figure 7C represents the 3D confocal scans from the constructs. Since each scan has a different layer number, it could be mistakenly deduced that the cell quantity is the same. We also noticed cell release from the construct under optical microscopy. The homogenous cell distribution inside the construct indicates a successful mixing process.

3.4. Gene expression

The RNA isolation resulted in a low nucleic acid yield; therefore, only five chondrogenesis marker genes were selected from previous research[5]. Figure 8 shows the changes in gene expressions. There were no significant alterations to the expressions of *COL1A1* and *COL10A1* during the investigated time. On the other hand, the expression of *COL2A1* increased during culture in the bioprinted construct, with a significant change after four weeks. It resulted in a high *COL2A1/COL1A1* ratio. In terms of transcription factor genes, *SOX9* and *RUNX2* expressions were higher after bioprinting but decreased
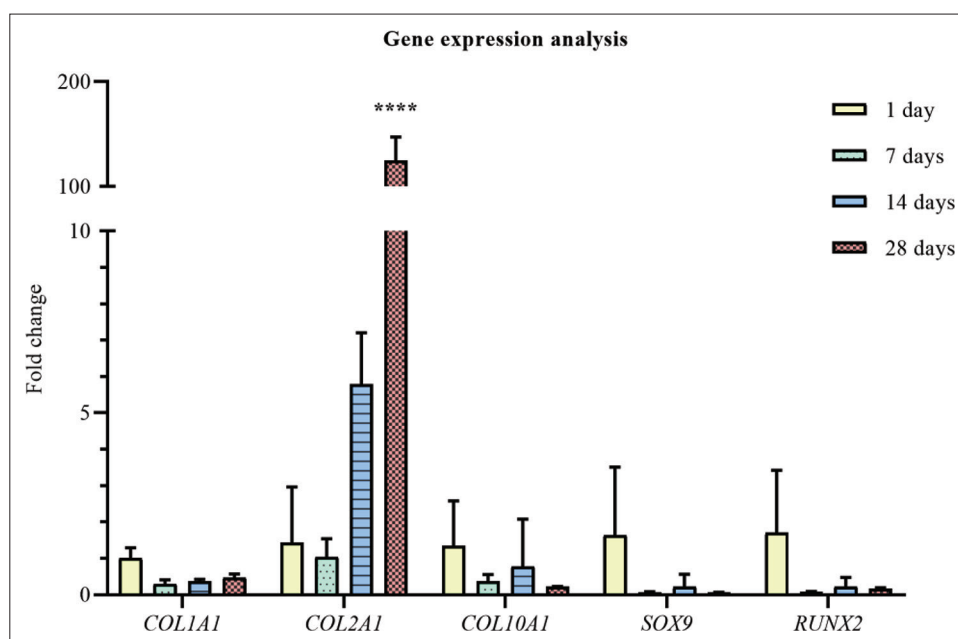
Figure 8. Gene expression analysis. There are only two biological replicates in 28-day group, while the number of replicates of other groups is indicated in Materials and methods. Note: ****$P < 0.0001$.

during culture in the construct; nonetheless, the change was statistically insignificant.

4. Discussion

This work focused on the formulation of a bioink composed of alginate, gelatin, and CCNC for meniscal 3D bioprinting. Rheological analysis enabled us to determine the optimal concentration of components.

Firstly, the temperature sweep test was performed to establish an optimal gelatin content, since gelatin contributes the most to the temperature-dependent rheological properties of bioinks[37,39]. The onset of a significant decrease in G' was observed for all bioinks at 28°C, which is closely related to the sol-gel transition temperature of gelatin[40,41]. Overall, gelatin is suitable for bioprinting at temperatures below 28°C[41,42]. These results imply that the bioink should be cooled to at least 25°C before bioprinting.

The shear-thinning behavior is another essential property of bioinks, which allows for precise and stable prints[43,44]. Bioink viscosities in the range of 30 mPa·s^{-1} to over $6·10^7$ mPa·s^{-1} are considered compatible for 3D extrusion bioprinting, and the viscosities of bioinks A, B, and C were within this range[45,46]. An increased concentration of gelatin stiffens the bioinks within the tested temperature range and ensures better printability and stability of bioprinted constructs. However, an excessive gelatin content may negatively affect the printing process due to nozzle clogging or non-uniform bioink flow. Higher viscosity also causes cellular damage; hence, bioinks with

low viscosity provide a cell-friendly environment for longer culturing periods although their printability is usually poor[47,48]. The amplitude sweep test proved that a lower gelatin content corresponded with the occurrence of cross-over at lower strain rates. Concomitantly, higher G' values were observed for bioinks with a higher gelatin content, which improves material strength but may result in poor printability[49]. Taking into account the entire viscosity range and the temperature sweep test, the composition of bioink B with a gelatin content of 4.0% has the most suitable rheological properties for 3D bioprinting and was chosen for further analysis. More precisely, the pivotal impact on this selection includes the broad LVE region, the reasonably high G' values, and the cross-over occurrence after a non-rapid decrease of the storage modulus of bioink B.

The amplitude sweep tests of bioinks with different alginate concentrations (bioinks B, D, and E) revealed the complexity of their viscoelastic properties and the inability to predict their properties solely from the concentrations of their constituents. The optimization of the alginate concentration is not only crucial for the printability and mechanical properties of the construct, but also for cell viability and proliferation[41,50]. Based on the rheological tests and the biological properties of alginate, the 0.75% alginate concentration was selected for further studies.

Lastly, the rheological dissimilarities between bioinks with different CCNC concentrations (bioinks D, F, and G) were assessed. This component has a significant impact on bioink reinforcement and the improvement of shear-

thinning behavior[51,52]. The CCNC concentration of 1.4% is optimal for preventing tears and clogs with higher values of the storage modulus and maintaining print integrity. From the rheological analysis, the selected bioink formulation is 4.0% gelatin, 0.75% alginate, and 1.4% CCNC.

We have formulated a printable bioink with the lowest shear stress and the highest printing accuracy by selecting the lowest possible concentration of components. The best printing accuracy was obtained with a 25 G nozzle for pressure below 55 kPa. This pressure is applicable for 3D bioprinting since higher pressures might increase shear stress in the nozzle and damage the cell membrane[53]. The shear forces exerted on cells may elicit alterations in the gene expression profile. Excess mechanical stress downregulates collagen type I and II expressions and upregulates matrix metallopeptidase (MMP) 1 and 13[24,54]. The MMPs encode collagenases that are involved in endochondral ossification or osteoarthritis through the degradation of ECM proteins, such as collagen type II and aggrecan. This situation is highly undesirable for cartilage tissue engineering. An attempt was made to perform a dynamic mechanical analysis (DMA 242 D, Netzsch) to compare the mechanical strength of the constructs; however, the scaffolds were too soft for the analyzer's detector (results not shown). We intended to repeat a dynamic mechanical analysis following the production of ECM proteins by cells. It is a feasible step since our bioprinted constructs were stable in culture medium for more than six months (results not shown). Another possibility is to enhance mechanical properties by introducing other materials, like PCL, as mentioned in the introduction[10,11,14].

Various crosslinking strategies may also be used to control the mechanical stress and bioprinting parameters. Gelatin with chemical modification can be subjected to enzymatic crosslinking to enable 3D bioprinting[55]. Besides, gelatin can be crosslinked with a chemical crosslinker, such as glutaraldehyde, which was used with a hydrogel composed of alginate, gelatin, and nanocellulose and compared with the Ca^{2+} alginate crosslinking[56]. Based on mechanical and structural differences, the divalent cation crosslinking of alginate was considered most suitable for 3D bioprinting. The selection of divalent ions and their concentration also influences the mechanical properties of alginate hydrogel; for example, strontium ions create more durable constructs than calcium ions[57]. Moreover, the proper use of cations can direct cell differentiation. Cobalt ions (Co^{2+}) mimic hypoxic conditions by inhibiting hypoxia-inducible factors[58]. Research performed on human mesenchymal stem cells encapsulated in alginate beads crosslinked with Co^{2+} revealed significant changes in cartilage-specific gene expression[59]. Live/dead assay and real-time PCR were performed to assess the biocompatibility of bioink. The high

cell viability within the bioprinted construct was observed at all time points. However, the decrease in cell count indicates that chondrocytes do not proliferate inside the construct, which is contrary to other research conducted on bioink composed of alginate and nanofibrillated cellulose[60]. In the future, the identification of proliferation markers, like Ki-67, should be carried out to prove the presence of proliferating cells[61]. The transcriptional control of the avascular meniscus phenotype is regulated by transcription factors SOX-9 and SOX-8 that upregulate $COL2\alpha1$, $COL11\alpha2$, and $ACAN$ expressions[62]. Products of these genes, namely collagen type II, type XI, and aggrecan, are the main structural proteins of the cartilaginous ECM. Endochondral ossification is a process in which bones replace the hyaline cartilage; hence, it is important to observe the expression of osteogenesis marker genes[63]. RUNX family transcription factor 2 (RUNX2) is the main transcription factor associated with osteogenesis. The change in $SOX9$ and $RUNX2$ expressions reduces $COL2\alpha1$ expression and initiates collagen type X synthesis, followed by increased collagen type I synthesis. Due to low yields of RNA extractions, only five genes' expressions were measured (Table 2). A significant change was observed only in the expression of $COL2A1$, which increased during the culture. The high accumulation of type II collagen is characteristic of the inner (white-white) and middle (white-red) zones of the meniscus[64]. However, collagen type I is still the most prevalent in the native meniscus. There were no observable significant changes in the rest of the analyzed genes. Perhaps, longer culture periods may allow for the observation of more significant changes.

The present study has several limitations. A good practice in bioink research is to conduct disintegration studies and pore size evaluation with the diffusion of nutrients[23]. The absence of these tests is due to the limited number of constructs, ensuing from the cells' low proliferative capacity and the high cell count required for 3D bioprinting, which is a challenge often underscored in the tissue engineering community[5,65,66]. Our team is also working on this issue (including 3D scaffold-free cultures and mesenchymal stem cell application).

Bioink with higher component concentrations (1.25% alginate, 20% gelatin, and 0.25% of cellulose nanofiber) was also proven succesful for meniscal bioprinting[7]. The viability of fibrochondorocytes was equally high (> 95 %). The most relevant differences were bioprinting with a wider nozzle (22 G) in comparison to the results presented in this study (25 G). The other bioink composed of 4% alginate, 35% gelatine, and 2% carboxymethyl cellulose was also succesfully used for extrusion into the negative mould[67]. Encapsulated MG-63 osteosarcoma cells proliferated and produced collagen inside the construct.

Finally, bioinks based on alginate, gelatine, and nanocellulose have also been extensively investigated for bone tissue engineering. Besides enhancing printability, cellulose also increases the expression of the osteogenic marker gene[22,68]. Dutta et al. observed notable gene expression changes; however, the mesenchymal stem cells were seeded on the construct composed of 3% alginate, 4% gelatin, and 1% cellulose nanocrystals rather than being encapsulated inside the bioink[68]. Nevertheless, only osteogenic-specific genes were studied. Finally, a comparable bioink formulation of 2.0% alginate, 3.3% gelatin, and 0.93% diethylaminoethyl cellulose was used for skin bioprinting, yielding promising results[69,70]. These studies suggest that the proposed bioink could be used for other 3D bioprinting applications.

5. Conclusion

This study presents the formulation and evaluation of a bioink dedicated to extrusion-based 3D bioprinting of meniscal tissue. The rheological analysis included the amplitude sweep test, temperature sweep test, and rotation. The selected bioink was used for bioprinting with normal human knee articular chondrocytes. Subsequently, the encapsulated cell viability and the gene expression of chondrogenic markers were investigated. In the course of rheological and biological analyses, we established an optimal bioink composition and proved that the bioink is printable, stable in cell culture, biocompatible, and able to maintain the native phenotype of chondrocytes. We intend to investigate the chondrogenic potential of bioink with human adipose-derived mesenchymal stem cells. In our ongoing research, the formulated bioink is used as a basis to promote the chondrogenesis of encapsulated cells through supplementation with hyaluronic acid, carbon nanotubes, or collagen and alterations in alginate crosslinking.

Acknowledgments

Funding

Conflict of interest

The authors declare no conflicts of interest.

Author contributions

Conceptualization: Julia Anna Semba, Adam Aron Mieloch, Jakub Dalibor Rybka
Investigation: Julia Anna Semba, Ewa Tomaszewska, Piotr Cywoniuk
Methodology: Julia Anna Semba, Adam Aron Mieloch
Supervision: Adam Aron Mieloch, Jakub Dalibor Rybka
Writing – original draft: Julia Anna Semba
Writing – review & editing: Adam Aron Mieloch, Jakub Dalibor Rybka

References

1. Pereira H, Varatojo R, Sevivas N, *et al.,* 2016, Physiopathology of the meniscal lesions, in: *Surgery of the Meniscus*, Springer Berlin Heidelberg, 47–61.

   https://doi:10.1007/978-3-662-49188-1_5

2. Doral MN, Bilge O, Huri G, *et al.*, 2018, Modern treatment of meniscal tears. *EFORT Open Rev*, 3:260–268.

   https://doi.org/10.1302/2058-5241.3.170067

3. Beaufils P, Becker R, Kopf S, *et al.*, 2017, The knee meniscus: Management of traumatic tears and degenerative lesions. *EFORT Open Rev*, 2:195–203.

   https://doi.org/10.1302/2058-5241.2.160056

4. Vaishya R, Patralekh MK, Vaish A, *et al.*, 2018, Publication trends and knowledge mapping in 3D printing in orthopaedics. *J Clin Orthop Trauma*, 9:194–201.

   https://doi.org/10.1016/j.jcot.2018.07.006

5. Semba JA, Mieloch AA, Rybka JD, 2020, Introduction to the state-of-the-art 3D bioprinting methods, design, and applications in orthopedics. *Bioprinting*, 18:e00070.

   https://doi.org/10.1016/j.bprint.2019.e00070

6. Agarwal S, Saha S, Balla VK, *et al.,* 2020, Current developments in 3D bioprinting for tissue and organ regeneration–A review. *Front Mech Eng*, 6:589171.

   https://doi.org/10.3389/fmech.2020.589171

7. Luo W, Song Z, Wang Z, *et al.*, 2020, Printability optimization of gelatin-alginate bioinks by cellulose nanofiber modification for potential meniscus bioprinting. *J Nanomater*.

   https://doi.org/10.1155/2020/3863428

8. Stanco D, Urbán P, Tirendi S, *et al.*, 2020, 3D bioprinting for orthopaedic applications: Current advances, challenges and regulatory considerations. *Bioprinting*, 20:e00103.

   https://doi.org/10.1016/j.bprint.2020.e00103

9. Ma X, Liu J, Zhu W, *et al.*, 2018, 3D bioprinting of functional tissue models for personalized drug screening and in vitro disease modeling. *Adv Drug Deliv Rev*, 132:235–251.

   https://doi.org/10.1016/j.addr.2018.06.011

10. Chae S, Lee SS, Choi YJ, *et al.*, 2021, 3D cell-printing of biocompatible and functional meniscus constructs using meniscus-derived bioink. *Biomaterials*, 267:120466.

https://doi.org/10.1016/j.biomaterials.2020.120466

11. Jian Z, Zhuang T, Qinyu T, *et al.*, 2021, 3D bioprinting of a biomimetic meniscal scaffold for application in tissue engineering. *Bioact Mater*, 6:1711–1726.

https://doi.org/10.1016/j.bioactmat.2020.11.027

12. Mieloch AA, Semba JA, Rybka JD, 2022, CNT-type dependent cellular adhesion on 3D-printed nanocomposite for tissue engineering. *Int J Bioprint*, 8(2):548.

https://doi.org/10.18063/ijb.v8i2.548

13. Vahedi P, Jarolmasjed S, Shafaei H, *et al.*, 2019, In vivo articular cartilage regeneration through infrapatellar adipose tissue derived stem cell in nanofiber polycaprolactone scaffold. Tissue and Cell 57:49–56.

https://doi.org/10.1016/j.tice.2019.02.002

14. Romanazzo S, Vedicherla S, Moran C, *et al.*, 2018, Meniscus ECM-functionalised hydrogels containing infrapatellar fat pad-derived stem cells for bioprinting of regionally defined meniscal tissue. J *Tissue Eng Regen Med*, 12:e1826–e1835.

https://doi.org/10.1002/term.2602

15. Saldin LT, Cramer MC, Velankar SS, *et al.*, 2017, Extracellular matrix hydrogels from decellularized tissues: Structure and function. *Acta Biomaterialia* 49:1–15

16. Ng WL, Chua CK, Shen YF, 2019, Print me an organ! Why we are not there yet. *Prog Polym Sci*, 97:101145.

https://doi.org/10.1016/j.progpolymsci.2019.101145

17. Liu D, Nikoo M, Boran G, *et al.*, 2015, Collagen and gelatin. Annu Rev Food Sci Technol, 6:527–557.

https://doi.org/10.1146/annurev-food-031414-111800

18. Ojansivu M, Rashad A, Ahlinder A, *et al.*, 2019, Wood-based nanocellulose and bioactive glass modified gelatin-alginate bioinks for 3D bioprinting of bone cells. *Biofabrication*, 11:35010.

https://doi.org/10.1088/1758-5090/ab0692

19. Leite ÁJ, Sarker B, Zehnder T, *et al.*, 2016, Bioplotting of a bioactive alginate dialdehyde-gelatin composite hydrogel containing bioactive glass nanoparticles. *Biofabrication*, 8:035005.

https://doi.org/10.1088/1758-5090/8/3/035005

20. Costantini M, Idaszek J, Szöke K, *et al.*, 2016, 3D bioprinting of BM-MSCs-loaded ECM biomimetic hydrogels for in vitro neocartilage formation. *Biofabrication*, 8:035002.

https://doi.org/10.1088/1758-5090/8/3/035002

21. Markstedt K, Mantas A, Tournier I, *et al.*, 2015, 3D bioprinting human chondrocytes with nanocellulose-alginate bioink for cartilage tissue engineering applications. *Biomacromolecules*, 16:1489–1496.

https://doi.org/10.1021/acs.biomac.5b00188

22. Ojansivu M, Rashad A, Ahlinder A, *et al.*, 2019, Wood-based nanocellulose and bioactive glass modified gelatin-alginate bioinks for 3D bioprinting of bone cells. *Biofabrication*, 11:035010.

https://doi.org/10.1088/1758-5090/ab0692

23. Zaeri A, Cao K, Zhang F, *et al.*, 2022, A review of the structural and physical properties that govern cell interactions with structured biomaterials enabled by additive manufacturing. *Bioprinting*, 26:e00201.

https://doi.org/10.1016/j.bprint.2022.e00201

24. Zhao Z, Li Y, Wang M, *et al.*, 2020, Mechanotransduction pathways in the regulation of cartilage chondrocyte homoeostasis. *Journal of Cellular and Molecular Medicine*, 24:5408–5419.

https://doi.org/10.1111/jcmm.15204

25. Möller T, Amoroso M, Hägg D, *et al.*, 2017, In vivo chondrogenesis in 3D bioprinted human cell-laden hydrogel constructs. *Plast Reconstr Surg—Glob Open*, 5:e1227.

https://doi.org/10.1097/GOX.0000000000001227

26. Jiang T, Munguia-Lopez JG, Flores-Torres S, *et al.*, 2019, Extrusion bioprinting of soft materials: An emerging technique for biological model fabrication. *Appl Phys Rev*, 6:011310.

https://doi.org/10.1063/1.5059393

27. Dravid A, McCaughey-Chapman A, Raos B, *et al.*, 2022, Development of agarose-gelatin bioinks for extrusion-based bioprinting and cell encapsulation. *Biomed Mater* (Bristol), 17:055001.

https://doi.org/10.1088/1748-605X/ac759f

28. Li Z, Huang S, Liu Y, *et al.*, 2018, Tuning alginate-gelatin bioink properties by varying solvent and their impact on stem cell behavior. *Sci Rep*, 8:8020.

https://doi.org/10.1038/s41598-018-26407-3

29. Zhuang P, Ng WL, An J, *et al.*, 2019, Layer-by-layer ultraviolet assisted extrusion-based (UAE) bioprinting of hydrogel constructs with high aspect ratio for soft tissue engineering applications. *PLoS ONE*, 14:1–21.

https://doi.org/10.1371/journal.pone.0216776

30. Zaeri A, Zgeib R, Cao K, *et al.*, 2022, Numerical analysis on the effects of microfluidic-based bioprinting parameters on the microfiber geometrical outcomes. *Sci Rep*, 12:1–16.

https://doi.org/10.1038/s41598-022-07392-0

31. Li X, Liu B, Pei B, *et al.*, 2020, Inkjet bioprinting of biomaterials. *Chem Rev*, 120:10793–10833.

https://doi.org/10.1021/acs.chemrev.0c00008

32. Ng WL, Huang X, Shkolnikov V, *et al.*, 2022, Controlling droplet impact velocity and droplet volume: key factors to achieving high cell viability in sub-nanoliter droplet-based bioprinting. *Int J Bioprint*, 8:424.

https://doi.org/10.18063/ijb.v8i1.424

33. Xiong R, Zhang Z, Chai W, *et al.*, 2017, Study of gelatin as an effective energy absorbing layer for laser bioprinting. *Biofabrication*, 9:024103.

https://doi.org/10.1088/1758-5090/aa74f2

34. Ng WL, Lee JM, Zhou M, *et al.*, 2020, Vat polymerization-based bioprinting—process, materials, applications and regulatory challenges. *Biofabrication*, 12:022001.

https://doi.org/10.1088/1758-5090/ab6034

35. Li W, Mille LS, Robledo JA, *et al.*, 2020, Recent advances in formulating and processing biomaterial inks for vat polymerization-based 3D printing. *Adv Healthc Mater*, 9:1–18.

https://doi.org/10.1002/adhm.202000156

36. Pääkkönen T, Dimic-Misic K, Orelma H, *et al.*, 2016, Effect of xylan in hardwood pulp on the reaction rate of TEMPO-mediated oxidation and the rheology of the final nanofibrillated cellulose gel. *Cellulose*, 23:277–293.

https://doi.org/https://doi.org/10.1007/s10570-015-0824-7

37. Jessop ZM, Al-Sabah A, Gardiner MD, *et al.,* 2017, 3D bioprinting for reconstructive surgery: Principles, applications and challenges. *J Plast Reconstr Aesthetic Surg*, 70(9):1155–1170.

https://doi.org/10.1016/j.bjps.2017.06.001

38. Giuseppe M di, Law N, Webb B, *et al.*, 2018, Mechanical behaviour of alginate-gelatin hydrogels for 3D bioprinting. *J Mech Behav Biomed Mater*, 79:150–157.

https://doi.org/10.1016/j.jmbbm.2017.12.018

39. Ning L, Gil CJ, Hwang B, *et al.*, 2020, Biomechanical factors in three-dimensional tissue bioprinting. *Appl Phys Rev*, 7:041319.

https://doi.org/10.1063/5.0023206

40. Kawabe S, Seki M, Tabata H, 2014, Investigation of the sol-gel transition of gelatin using terahertz time-domain spectroscopy. *J Appl Phys*, 115:143103.

https://doi.org/10.1063/1.4870954

41. Liu F, Chen Q, Liu C, *et al.*, 2018, Natural polymers for organ 3D bioprinting. *Polymers (Basel)*, 10:1278.

https://doi.org/10.3390/polym10111278

42. Kačarević ŽP, Rider PM, Alkildani S, *et al.*, 2018, An introduction to 3D bioprinting: Possibilities, challenges and future aspects. *Materials*, 11:2199.

https://doi.org/10.3390/ma11112199

43. Dimitreli G, Thomareis AS, 2004, Effect of temperature and chemical composition on processed cheese apparent viscosity. *J Food Eng*, 64:265–271.

https://doi.org/10.1016/j.jfoodeng.2003.10.008

44. Li MG, Tian XY, Chen XB, 2009, A brief review of dispensing-based rapid prototyping techniques in tissue scaffold fabrication: Role of modeling on scaffold properties prediction. *Biofabrication*, 1:032001.

https://doi.org/10.1088/1758-5082/1/3/032001

45. Murphy S V., Atala A, 2014, 3D bioprinting of tissues and organs. *Nat Biotechnol*, 32:773–785.

https://doi.org/10.1038/nbt.2958

46. Jones N, 2012, Science in three dimensions: The print revolution. *Nature*, 487:22–23.

https://doi.org/10.1038/487022a

47. Rutz AL, Hyland KE, Jakus AE, *et al.*, 2015, A multimaterial bioink method for 3D printing tunable, cell-compatible hydrogels. *Adv Mater*, 27:1607–1614.

https://doi.org/10.1002/adma.201405076

48. Blaeser A, Duarte Campos DF, Puster U, *et al.*, 2016, Controlling shear stress in 3D bioprinting is a key factor to balance printing resolution and stem cell integrity. *Adv Healthc Mater*, 5:326–333.

https://doi.org/10.1002/adhm.201500677

49. Jin Y, Zhao D, Huang Y, 2018, Study of extrudability and standoff distance effect during nanoclay-enabled direct printing. *Bio-Des Manuf*, 1:123–134.

https://doi.org/10.1007/s42242-018-0009-y

50. Markstedt K, Mantas A, Tournier I, *et al.*, 2015, 3D bioprinting human chondrocytes with nanocellulose-alginate bioink for cartilage tissue engineering applications. *Biomacromolecules*, 16:1489–1496.

https://doi.org/10.1021/acs.biomac.5b00188

51. Athukoralalage SS, Balu R, Dutta NK, *et al.,* 2019, 3D bioprinted nanocellulose-based hydrogels for tissue engineering applications: A brief review. *Polymers*, 11(5):898.

https://doi.org/10.3390/polym11050898

52. Han C, Wang X, Ni Z, *et al.*, 2020, Effects of nanocellulose on alginate/gelatin bio-inks for extrusion-based 3D printing. *BioResources*, 15:7357–7373.

https://doi.org/10.15376/biores.15.4.7357-7373

53. Fakhruddin K, Hamzah MSA, Razak SIA, 2018, Effects of extrusion pressure and printing speed of 3D bioprinted construct on the fibroblast cells viability. *IOP Conf Ser: Mater Sci Eng*, 440:012042.

https://doi.org/10.1088/1757-899X/440/1/012042

54. Liu Q, Hu X, Zhang X, *et al.*, 2016, Effects of mechanical stress on chondrocyte phenotype and chondrocyte extracellular matrix expression. *Sci Rep*, 6:1–8.

https://doi.org/10.1038/srep37268

55. He H, Li D, Lin Z, *et al.*, 2020, Temperature-programmable and enzymatically solidifiable gelatin-based bioinks enable facile extrusion bioprinting. *Biofabrication*, 12.

https://doi.org/10.1088/1758-5090/ab9906

56. Erkoc P, Uvak I, Nazeer MA, *et al.*, 2020, 3D printing of cytocompatible gelatin-cellulose-alginate blend hydrogels. *Macromol Biosci*, 20:1–15.

https://doi.org/10.1002/mabi.202000106

57. Place ES, Rojo L, Gentleman E, *et al.*, 2011, Strontium-and zinc-alginate hydrogels for bone tissue engineering. *Tissue Eng Part A*, 17:2713–2722.

https://doi.org/10.1089/ten.tea.2011.0059

58. Teti G, Focaroli S, Salvatore V, *et al.*, 2018, The hypoxia-mimetic agent cobalt chloride differently affects human mesenchymal stem cells in their chondrogenic potential. *Stem Cells Int*, 2018: 3237253.

https://doi.org/10.1155/2018/3237253

59. Focaroli S, Teti G, Salvatore V, *et al.*, 2016, Calcium/cobalt alginate beads as functional scaffolds for cartilage tissue engineering. *Stem Cells Int*, 2016:20–22.

https://doi.org/10.1155/2016/2030478

60. Nguyen D, Hgg DA, Forsman A, *et al.*, 2017, Cartilage tissue engineering by the 3D bioprinting of iPS cells in a nanocellulose/alginate bioink. *Sci Rep*, 7:658.

https://doi.org/10.1038/s41598-017-00690-y

61. Apelgren P, Amoroso M, Lindahl A, *et al.*, (2017) Chondrocytes and stem cells in 3D-bioprinted structures create human cartilage in vivo. *PLoS ONE*, 12:e0189428.

https://doi.org/10.1371/journal.pone.0189428

62. Grogan SP, Duffy SF, Pauli C, *et al.*, 2018, Gene expression profiles of the meniscus avascular phenotype: A guide for meniscus tissue engineering. *J Orthop Res*, 36:1947–1958.

https://doi.org/10.1002/jor.23864

63. Mackie EJ, Ahmed YA, Tatarczuch L, *et al.*, 2008, Endochondral ossification: how cartilage is converted into bone in the developing skeleton. *Int J Biochem Cell Biol*, 40:46–62.

https://doi.org/10.1016/j.biocel.2007.06.009

64. Folkesson E, Turkiewicz A, Rydén M, *et al.*, 2020, Proteomic characterization of the normal human medial meniscus body using data-independent acquisition mass spectrometry. *J Orthop Res*, 38:1735–1745.

https://doi.org/10.1002/jor.24602

65. Francis SL, di Bella C, Wallace GG, *et al.*, 2018, Cartilage tissue engineering using stem cells and bioprinting technology—barriers to clinical translation. *Front Surg*, 5:1–12.

https://doi.org/10.3389/fsurg.2018.00070

66. Sharma P, Kumar P, Sharma R, *et al.*, 2019, Tissue engineering; current status & futuristic scope. *J Med Life*, 12:225–229.

https://doi.org/10.25122/jml-2019-0032

67. Sathish PB, Gayathri S, Priyanka J, *et al.*, 2022, Tricomposite gelatin-carboxymethylcellulose-alginate bioink for direct and indirect 3D printing of human knee meniscal scaffold. *Int J Biol Macromol*, 195:179–189.

https://doi.org/10.1016/j.ijbiomac.2021.11.184

68. Dutta SD, Hexiu J, Patel DK, *et al.*, 2021, 3D-printed bioactive and biodegradable hydrogel scaffolds of alginate/gelatin/cellulose nanocrystals for tissue engineering. *Int J Biol* Macromol, 167:644–658.

https://doi.org/10.1016/j.ijbiomac.2020.12.011

69. Ramakrishnan R, Kasoju N, Raju R, *et al.*, 2022, Exploring the potential of alginate-gelatin-diethylaminoethyl cellulose-fibrinogen based bioink for 3d bioprinting of skin tissue constructs. *Carbohydr Polym Technol Appl*, 3:100184.

https://doi.org/10.1016/j.carpta.2022.100184

70. Somasekharan LT, Raju R, Kumar S, *et al.*, 2021, Biofabrication of skin tissue constructs using alginate, gelatin and diethylaminoethyl cellulose bioink. *Int J Biol* Macromol, 189:398–409.

https://doi.org/10.1016/j.ijbiomac.2021.08.114